Comments on Inorganic Chemistry
Publication details, including instructions for authors and subscription information:
http://www.informaworld.com/smpp/title~content=t713455155

METAL CHALCOGENIDE GELS, XEROGELS AND AEROGELS

Stephanie L. Brock[a]; Indika U. Arachchige[a]; Kennedy K. Kalebaila[a]
[a] Department of Chemistry, Wayne State University, Detroit, Michigan, USA

To cite this Article Brock, Stephanie L. , Arachchige, Indika U. and Kalebaila, Kennedy K.(2006) 'METAL CHALCOGENIDE GELS, XEROGELS AND AEROGELS', Comments on Inorganic Chemistry, 27: 5, 103 — 126
To link to this Article: DOI: 10.1080/02603590601084434
URL: http://dx.doi.org/10.1080/02603590601084434

Comments on Inorganic Chemistry, 27: 103–126, 2006

ISSN: 0260-3594 print
DOI: 10.1080/02603590601084434

Taylor & Francis
Taylor & Francis Group

METAL CHALCOGENIDE GELS, XEROGELS AND AEROGELS

STEPHANIE L. BROCK
INDIKA U. ARACHCHIGE
KENNEDY K. KALEBAILA

Department of Chemistry, Wayne State University, Detroit, Michigan, USA

Metal chalcogenide gels represent an intriguing class of nanostructured solids that are largely unexplored, in contrast to oxides. This Comment reviews the two synthetic approaches applied for gelation of metal chalcogenides—thiolysis and nanoparticle condensation—and presents a survey of the materials prepared by these strategies. Drying strategies to produce dense xerogels (ambient pressure) and highly porous aerogels (supercritical fluid extraction) are described and the effect of density on the extent of quantum confinement in semiconducting metal chalcogenide gel structures is discussed.

INTRODUCTION

Despite strong current interest in nanostructured materials, particularly with respect to chalcogenide semiconductors (e.g., CdSe, $CuInS_2$, PbTe, etc.), metal chalcogenide gels—porous frameworks of metal chalcogenides—remain a largely unexplored area of investigation. However, this expanding class of materials has the potential to address a number of issues that impact the implementation of semiconductor nanomaterials in functional devices. Of particular interest is the fact that the primary components of the gels are in the size regime where quantum

Address correspondence to Stephanie L. Brock, Department of Chemistry, Wayne State University, Detroit, MI 48202, USA. E-mail: sbrock@chem.wayne.edu

confinement effects are noted.[1] Quantum confinement effects arise when the Bohr radius of the exciton (the electron-hole pair formed upon excitation) is smaller than the radius of the particles. The consequence is an apparent increase in the bandgap for a semiconductor material as the size is decreased below this critical radius. This results in a blue-shift of the absorbance/luminescence spectra that can be tuned as a function of the particle size. Applications for such materials in solid state devices are largely limited by a dearth of methodologies for assembling particles into 2-D or 3-D architectures without compromising the unique opto-electronic characteristics of the nanoscale building blocks. Commonly employed colloidal crystallization techniques can produce ordered arrays of particles, but each is spatially isolated by its ligand sphere, i.e., the particles are not physically connected.[2] Or, if they are connected, it is through heterogenous ligation, not through intimate contact between the nanoparticle components. One tried and true methodology for generating homogeneous nanonetworks, well explored for oxides, is the sol-gel approach.

Equally important to the "substance" of the gel (the nanonetwork) is the presence of an interconnected pore structure consisting of micro (< 2 nm), meso (2–50 nm), and macro (>50 nm) pores. In wet gels, the pores are filled with solvent, whereas in the "dried" forms—xerogels and aerogels—the pores are filled with gas.[3] Aerogels retain most of the pore characteristics of the wet gels, whereas xerogels are considerably compacted, and have correspondingly smaller pores and a lower total pore volume. The porosity characteristics have been exploited for catalysis, immobilization, sensing, and electrochemical applications, i.e., any applications where maximizing a solid-gas or solid-liquid interface is important.[4] Additionally, the formation of porous structures or particles is important in ceramic manufacture, since the initial pore structure or particle size/polydispersity is a strong determiner of the quality of the prepared ceramic.[3]

To date, sol-gel approaches for generation of inorganic materials have been focused largely on oxides, traditionally, insulating or wide-band gap semiconductors, and more recently, electronically conductive oxides.[4,5] Metal chalcogenide analogs would address a whole host of applications that are not suitably addressed by their oxide counterparts. The ability to tune the band gap of semiconducting chalcogenides throughout the visible region within a chemically accessible porous architecture opens up possibilities for photocatalytic and sensing applications. Additionally, metal chalcogenides are favored over oxides

as IR-transparent glasses (GeS_2, ZnS)[6,7] and are also being investigated as cathode materials in Li-ion batteries (TiS_2).[8,9]

This Comment will describe the current state of the science for metal chalcogenide gels, xerogels, and aerogels. To put this work into context, the traditional sol-gel process, as applied to oxides, will be briefly described. Subsequently, two processes for metal chalcogenide gel formation, thiolysis and nanoparticle condensation, will be discussed. The properties of the resultant chalcogenide gels, and the recent application of these methods for aerogel and xerogel formation, will be described and the consequences of network density on quantum confinement effects discussed.

THE SOL-GEL PROCESS

Sol-gel methods are extensively used in the formation of metal oxide ceramics, glasses, and porous materials, and typically follow a route based on the hydrolysis and condensation of molecular precursors, although routes based on inorganic salts or colloid aggregation may also be used.[4] Hydrolysis of metal alkoxides results in the formation of hydroxylated metal centers, which can then undergo condensation, ultimately producing a wet gel network.[4,5] For silica, the best-studied system, the sol gel process can be catalyzed either by an acid or a base, with the type of catalyst dictating the rate of hydrolysis and condensation. In the case of acid catalyzed sol gel reactions, a large number of reactive hydroxylated species are formed simultaneously, resulting in a polymer-like gel with small pores. However, under basic conditions, condensation is favored, yielding a particulate gel having an interconnected network of particles with large pores.

When dried under ambient conditions, gels undergo capillary collapse, resulting in significant densification and xerogel formation. In ceramic and glass processing, densification is a desired process; however, for applications involving catalysis and sensing, high surface areas are ideal. To retain the wet gel structure (i.e., produce an aerogel), a number of techniques have been employed. Kistler discovered that supercritical fluid drying of wet gels preserved the pore structure because of the absence of a liquid-gas interface, and this is still the most common technique for aerogel production.[10,11] If alcohols are used as the solvent, high temperatures are required to achieve a supercritical state; hence, CO_2 is often used instead, permitting extraction at temperatures of ca. 35°C. Alternatively, ambient

drying techniques, in which the gel surface is coated with non-reactive groups to prevent silica condensation, thus allowing the gel to "spring-back" after drying, or in which the gel is dried from a non-polar solvent that has only weak interactions with the highly polar pore walls, can be performed to retain a good measure of the porosity.[4]

During the last two decades, scientists have begun to extend the sol-gel method to non–oxide systems, including metal nitrides and chalcogenides.[12] Two general approaches are followed for the preparation of metal chalcogenides, the subject of this Comment. In thiolysis, a metal complex (often an alkoxide) is reacted with H_2S or a similar sulfiding agent, whereas in the nanoparticle condensation (colloid aggregation) strategy, metal chalcogenide nanoparticles are produced in a separate step, and then condensed together.

I. THIOLYSIS STRATEGIES

When gaseous H_2S is employed in a sol-gel reaction in lieu of H_2O, metal sulfide powders or gels can arise. Representative thiolysis and condensation steps are presented for the reaction of $Ge(OEt)_4$ with H_2S in Equations (1) and (2), respectively. Repetition of these steps ultimately leads to formation of GeS_2.

$$Ge(OEt)_4 + xH_2S \rightarrow Ge(OEt)_{4-x}(SH)_x + xHOEt \quad (1)$$

$$2Ge(OEt)_{4-x}(SH)_x \rightarrow (EtO)_{4-x}(HS)_{x-1}Ge-S-Ge(SH)_{x-1}(OEt)_{4-x} + H_2S \quad (2)$$

Thiolysis reactions have been reported for the preparation of a number of metal sulfide gels, xerogels, and ceramics. The question of whether a gel or precipitate results is strongly dependent on the synthetic conditions employed. Another complication is the potential for oxide contamination from incomplete thiolysis of alkoxide precursors. For this reason, a number of researchers have turned to precursors where no metal-oxygen bond is present, including thiolates, silylamides and metal akyls. Sulfur sources other than H_2S have also been investigated. Although not technically "thiolysis" reactions, they are included here because the reactions are presumed to occur by a similar mechanism and have been demonstrated to lead to gelation. Thiolysis sol-gel routes have focused primarily on formation of dense metal sulfide materials (glasses and ceramics).

Sulfides of La, Ca-Y, Ti, Nb, Mo, W, Re, Ni, Zn

An overview of the gels and precipitates prepared using thiolysis strategies is presented in Table 1 and discussed below. GeS_2 (not listed) is discussed in detail a separate section.

Kumta and co-workers have reported the synthesis of TiS_2, NbS_2 and La_2S_3 phases from thiolysis reactions of the respective metal alkoxides. The as-prepared products were amorphous or poorly crystalline and contained oxides, which could be eliminated by annealing at high temperatures (800–1000°C) under flowing H_2S to yield highly crystalline single-phase metal sulfides.[9,13–15] Reactions of $Ti(OPr^i)_4$ with the alternate sulfur sources dimethyldisulfide and hexamethyldisilthiane were also explored; however, the sulfur contents of the amorphous as-prepared products were lower than those achieved with H_2S, suggesting replacement of alkoxy groups by sulfur for these agents is less facile.[9] To avoid oxide formation altogether, Carmalt and her colleagues explored thiolate precursors such as $[Ti(SBu^t)_4]$ and $[Nb(SC_6H_3Me_2\text{-}2,6)_5]$. In the case of titanium, crystalline sulfides, TiS_2 and $Ti_{1.25}S_2$, could be prepared without oxide contamination by annealing at 600°C in flowing H_2S.[8] Thiolysis of the niobium thiolate precursor followed by heating of the resultant precipitate under flowing H_2S at 750°C yielded crystalline NbS_2,[16] similar to the product obtained by thiolysis of $Nb(OEt)_5$.[9] Likewise, Allen et al. turned to silylamides, such as $La(N(tms)_2)_3$ (tms = trimethylsilyl), which yielded LaS_2-type phases upon heating at 500°C under flowing H_2S.[17]

Thiolates and silylamides have also been investigated for the preparation of ternary sulfides of yttrium with alkaline earth metals. Purdy and co-workers evaluated thiolysis reactions of $Y(N(tms)_2)_3$ and $(Y(SCEt_3)_3py_2)_2$ with alkaline earth metal thiolates (e.g., $Ca(SCMe_3)_2$).[18] Thiolysis led to powder or gel-like precipitates that were pressed into pellets and annealed under flowing H_2S. Although they were able to successfully make phases such as CaY_2S_4 and SrY_2S_4, a variety of IR absorbing impurities remained trapped in the matrices, making these materials unsuitable for optical applications.[18]

Stanić and co-workers have focused predominantly on alkoxide precursors for sulfides of zinc and tungsten. They obtained a yellow semi-transparent ZnS gel when H_2S was bubbled through a solution of $Zn(OBu^t)_2$ in toluene, which dried into a red-orange solid (xerogel) consisting of crystallites of ca 10 nm in size (determined from powder

Table 1. Metal sulfide formation by thiolysis reactions

Metal	Metal Precursor	Sulfur Precursor	Products and References
La	$La(OPr^i)_4$, $La(NO_3)_3{\cdot}6H_2O$	H_2S, $S(Bu^t)_2$	Amorphous ppt; 1000°C in $H_2S = La_2S_3$[13,14]
	$La(N(tms)_2)_3$	H_2S	Amorphous gel, 510°C in $H_2S = LaS_x$, $x < 2$[17]
AE-Y (AE = Ca, Sr)	$AE(SCEt_3)_2$, $Y(SCEt_3)_3$, $Y(N(tms)_2)_3$	H_2S	1000–1100°C in $H_2S = CaY_2S_4$, SrY_2S_4 (1AE:2Y); $= Th_3P_4$-type Ca-Y-S (1Ca:3.5Y)[18]
Ti	$Ti(OR)_4$, R = Pr^i, Et, Bu, EHO	H_2S, MeS-SMe, $S(tms)_2$	Amorphous ppt; 600°C in $H_2S = TiS_2 + TiO_2$; 800°C in $H_2S = TiS_2$[9]
	$Ti(SBu^t)_4$	H_2S	Amorphous ppt; 600°C in $H_2S = TiS_2 + Ti_{1.25}S_2$[8]
Nb	$Nb(OEt)_5$	H_2S	Amorphous ppt; 700°C in $H_2S = NbS_2$[9]
	$Nb(SC_6H_3Me_2 - 2,6)_5$	H_2S	Amorphous ppt; 750°C in $H_2S = NbS_2$[16]
Mo	$Mo(O)(OMe)_4$	$HC(S)NMe_2$	Crystalline MoS_2 ppt[20]
W	$W(OEt)_6$	H_2S	Amorphous WS_x, $x = 1.4$, gel[19]
	$WCl_2(OEt)_3$	H_2S	Amorphous WS_x, $x = 2.7$, aggregate (ppt)[19]
	$W(O)(OMe)_4$	$HC(S)NMe_2$	Crystalline WS_3 ppt[20]
Re	Re_2O_7	$HC(S)NMe_2$	Crystalline Re_2S_7 ppt[20]
Ni	$Ni(acac)_2$,	$HC(S)NMe_2$	NiS (EDS data) ppt[20]
	$Ni(O(CH(Me)CH_2NMe_2))_2$	$HC(S)NMe_2$	NiS (EDS data) ppt[20]
Zn	$Zn(acac)_2$	$HC(S)NMe_2$,	ZnS (cubic) nanocrystallite aggregates (ppt)[20]
	$Zn(OBu^t)_2$	H_2S	ZnS (cubic) nanoparticulate gel[7]
	$Zn(Et)_2$	$(BzS)_2S$	Visually similar to $Zn(OBu^t)^2/H_2S$ gel[7]

EHO = 2-ethylhexoxide, tms = trimethylsilane, EDS = energy dispersive spectroscopy.

X-ray diffraction). When a saturated solution of H_2S was mixed with the precursor solutions, a polymeric gel was obtained, whereas a particulate gel was obtained when H_2S was continuously bubbled through the precursor solutions. A product similar in appearance was also obtained from the reaction of $ZnEt_2$ in toluene with dibenzyltrisulfide.[7] Amorphous tungsten sulfides were formed by thiolysis reactions of $W(OEt)_6$ and $WCl_2(OEt)_3$ in toluene. For $WCl_2(OEt)_3$, a nonstoichiometric colloidal powder, W:S (1:1.4), was obtained with a surface area of $3.5\,m^2/g$; whereas in the case of $W(OEt)_6$, a thixotropic particulate gel was obtained that dried at ambient conditions to give a xerogel with a ratio of W:S equal to 1:2.7.[19]

Kessler and co-workers have focused on the use the thiocarbonyl N, N-dimethylthioformamide for production of metal sulfides by sol-gel strategies. Reactions with molybdenum and tungsten oxoalkoxides, rhenium heptaoxide, and nickel or zinc acetylacetonates all yielded crystalline precipitates of the corresponding sulfides.[20]

Germanium Sulfide Gels, Xerogels and Thin Films

Among the sol-gel derived metal chalcogenides, GeS_2 has been the most extensively studied because of interest in glassy materials for IR windows, fibers, and planar waveguides.[6,21,22] In 1984, Melling reported the preparation of GeS_2 from $Ge(OEt)_4$ in anhydrous toluene via thiolysis.[6] However, subsequent work by Hodgson and co-workers revealed that the diffraction data of Melling is better attributed to crystalline hexagonal GeO_2, although IR analyses suggested a substantial portion of the product was GeS_2 (amorphous).[23] They concluded that the GeS_2 product reacts with H_2O on exposure to air or, alternatively, that there is a competing reaction to cleave bonds at O-Et rather than at Ge-O. Stanić and co-workers explored a variety of concentration ratios of $[H_2S]/[Ge(OEt)_4]$ in toluene, designated by R, and for $R = 2.5$ they obtained xerogels that exhibited unusually high surface areas ($491\,m^2/g$), rivaling those of the extensively studied silica xerogels and suggesting a robust pore network can be obtained in this system.[24,25,26] However, as-prepared GeS_2 was again found to be contaminated with GeO_2, attributed to moisture in the H_2S gas source. In efforts to reduce oxide contamination, Stanić and co-workers passed H_2S through concentrated H_2SO_4 to liberate elemental sulfur and carry it with the excess H_2S into the $Ge(OEt)_4$ solution, until a gel had formed. Although GeO_2 is clearly present in as-prepared gels, along with orthorhombic sulfur,

upon heating in vacuo at 630°C, only phase-pure GeS_2 was obtained. The authors postulate that the elemental sulfur embedded in the gel network reacts with GeO_2 to yield GeS_2 along with SO_2 as a gaseous byproduct.[27] Sanghera and colleagues followed a similar preparative procedure to that initially employed by Stanić and co-workers (i.e., without H_2SO_4), but they doped the reaction mixture with Er^{3+} and observed that gelation was quicker and thiolysis more complete than GeS_2 gelation by itself, based on the absence of Ge-OR bands in the IR spectra of as-prepared gels.[28] Martins and colleagues explored reactions of $GeCl_4$ and $Ge(OEt)_4$ with a variety of sulfur sources, including H_2S, thioacetamide and thiourea, to prepare thin films for planar waveguides. They found that elimination of oxide is best achieved in thin films produced from reaction of $GeCl_4$ with thioacetamide in ethanol; however, the resultant materials contain chloride impurities.[22]

Germanium Sulfide Aerogels

Kistler postulated that "the ability to form an aerogel is a general property of a gel."[11] However, this is a premise that has not been extensively tested outside of oxide materials. The Brock group is interested in probing whether thiolysis routes combined with low-temperature supercritical drying techniques are amenable to formation of metal sulfide aerogels, and in evaluating how these materials compare to oxides formed by hydrolysis reactions. Our initial foray into this area has been with GeS_2 aerogels. Intrigued by the extremely high surface areas achieved by GeS_2 xerogels (ca. $500\,m^2/g$), we sought to test whether supercritical drying could augment surface areas still further.

Germanium sulfide gels were synthesized according to that procedure of Stanić et al. whereby xerogels with the highest surface areas were reported.[25] Thiolysis of a non-aqueous solution of $Ge(OEt)_4$ ($R = 2.5$) yielded flocculant gels that were dried in vacuo (to form xerogels) and by supercritical fluid extraction (to create aerogels). Under these conditions, the reaction appears to proceed by fast nucleation and relatively slow condensation, creating a particulate gel, as illustrated in Figure 1.[29] The as-prepared GeS_x aerogels are amorphous, and exhibit surface areas of $755\,m^2/g$, far greater than the corresponding xerogels ($478\,m^2/g$), consistent with the expectation that the pore network is better preserved in supercritically dried samples. This is evident by comparison of TEM micrographs of aerogel and xerogel (Figure 1)

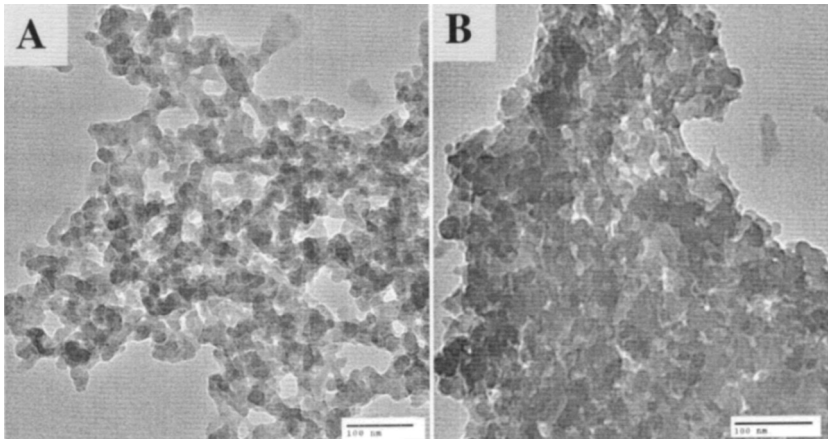

Figure 1. TEM images of a germanium sulfide aerogel (A) and xerogel (B) illustrating the effect of drying techniques on resultant porosity. Reproduced with permission from *J. Non-Cryst. Solids*, **352**, 232 (2006). Copyright 2006 Elsevier.

where the pores are clearly evident in the aerogel, whereas the xerogel forms a compact mass. When compared on a per mole basis, these surface areas are comparable to ultra low density silica aerogels ($>1200\,m^2/g$), which set the benchmark for highly porous inorganic materials. Interestingly, although the wet gel is very susceptible to oxidation (resulting in formation of crystalline GeO_2 at ambient temperatures), the dry gel appears to be quite stable.[29] It could be that mass transport is a requirement for crystal growth of GeO_2, and this can be achieved quite easily in solution, but not the solid state (at least not at ambient temperatures).

This study represents the first example of a metal sulfide aerogel prepared via a thiolysis route and supports Kistler's notion that the phenomenon of aerogel formation is general and potentially applicable to a wide range of systems.[11] We see no reason why the bulk of the metal chalcogenide gels prepared by thiolysis could not be transformed to aerogels with similarly large surface areas, providing the conditions of thiolysis are appropriately tuned to generate a gel and not a precipitate.

II. NANOPARTICLE CONDENSATION STRATEGIES

The nature of the gel (particulate or polymeric, strong or weak) is strongly determined by the reaction parameters. In thiolysis sol-gel

approaches, the relative rates of thiolysis and condensation dictate the structure of the resultant gel,[26] and the inability to control these rates can give rise to precipitates in lieu of the desired gel structure. One way to ensure that a particulate gel is formed (rather than a polymeric gel) is to separate the steps involving particle formation and condensation. Using now-routine methods to control the size and shape of nanoparticles, which typically involve coordinating solvents or microemulsions, a stable sol of nanoparticles can be prepared.[30] In a second step, these can be condensed together in a controlled fashion through destabilization of the resultant sol. This technique, applied to metal chalcogenides for the first time by Gacoin and co-workers in 1997,[31,32] is proving to be a versatile path for generating a wide range of metal chalcogenide gels, xerogels, and aerogels, as discussed below.

CdS Gels and Films

Colloidal CdS nanoparticles (quantum dots) have been transformed into transparent or opaque CdS wet gels by a two step strategy, as described by Gacoin and co-workers.[31–35] First, primary nanoparticles of CdS were formed from $Cd(NO_3)_2$ and H_2S, either using inverse microemulsion techniques followed by complexation with 4-fluorophenylthiolate, or by direct precipitation of particles in the presence of 4-fluorophenylthiol. The particles were subsequently dispersed in acetone to create a stable sol.[31] In the second step, destabilization of colloidal CdS nanoparticles leading to gel network formation was achieved by oxidative loss of 4-fluorophenylthiolate ligands from the nanoparticle surface using H_2O_2. ^{19}F NMR analyses of partially oxidized CdS sols have shown that the thiolates and their oxidized products (disulfides and sulfonates) are not part of the aggregates; i.e., the CdS nanoparticles are physically connected to each other without any organic linkers.[31–33,35] The oxidized thiol fraction ($X = 2[H_2O_2]/[FPhSH]$), which controls the number of active surface sites in the starting sol, is the key factor for the gelation process.[32] If the X value is too low ($X < 0.2$), depassivation is not achieved and the particles remain dispersed without aggregation.[33] Visual changes in the CdS sol (0.1 M with 2 nm colloids) were only observed when the value of X was greater than or equal to 0.2.[33] However, shrinkage ($X > 0.5$) or precipitation ($X > 1$) was observed in the presence of higher amounts of H_2O_2, attributed to large number of active sites that are formed on the nanoparticles' surfaces or within the wet gel

network.[33] Moreover, the amount of water present in the sol showed a remarkable effect on the aggregation rate, as it can solvate the byproducts of the oxidation.[33] The use of other common oxidants, such as bromine or benzoyl peroxide, resulted in the formation of large number of active sites on the nanoparticles' surfaces, which leads to rapid precipitation rather than gel formation.[33]

Gacoin also reports that there is no significant change in the absorption spectra during the aggregation of CdS colloids, indicating the average crystallite size remains essentially unchanged during the aggregation process (i.e., the nanoparticles exhibit the same degree of quantum confinement after gelation as before).[33] However, the use of higher amounts of H_2O_2 ($X > 0.8$ in 0.1 M, 2 nm CdS colloids) resulted in a blue shift of the absorption band as a result of partial dissolution of CdS nanoparticles. In addition to the formation of firm transparent gels, thin films were prepared by spin coating a mixture of the sol with polyvinyl-pyrrolidone, with the latter added to prevent crack formation. The films exhibited some degree of waveguiding, and optical absorbance and photoluminescence measurements confirm the quantum-confined nature of the CdS nanostructure.[34]

CdS Xerogels and Aerogels

We were intrigued by the observation that quantum confinement effects are retained in the CdS gels, even as the particles are connected into a 3-D monolithic solid. Generally, as the dimensionality of the nanoparticle system increases (i.e., from spherical particles, or "dots," to rods, wires, and planes) the extent of quantum confinement decreases for comparable lengthscales of the confined dimension.[36,37] This is because the exciton has more degrees of freedom in which to move as the dimensionality increases. Gel structures present an opportunity to explore the effects of intermediate, or fractal, dimensionalities on quantum confinement effects. In addition to potentially "conserving" quantum confinement effects in 3-D connected networks of nanoparticles, the porosity of the framework also permits the interaction of the gel with the outside world. The tunable bandgap and large interfacial surface area make these materials ideal for sensing, photocatalytic, and photovoltaic devices. Accordingly, we sought to test whether the pore structure of wet CdS gels could be retained in dried gels through supercritical drying (i.e., can a CdS

aerogel be prepared), and probed the effect of gel density on the extent of quantum confinement through comparison to analogous xerogels.

Nanoparticles were prepared by a modification of the Gacoin method employing sodium sulfide in lieu of H_2S. Gelation of a sol consisting of 4.5 nm diameter CdS particles (0.1 M [Cd]) was achieved by addition of H_2O_2. The gels were aged for up to a month, solvent exchanged several times to remove the oxidation byproducts, and then either dried on the benchtop under ambient conditions or supercritically with CO_2. The effect of drying on the material is immediately evident from visual comparison of a wet gel, xerogel, and aerogel (Figure 2A).[38,39] The aerogel exhibited only a 5–10% volume loss relative to the wet gel, whereas the xerogel exhibits ca. 90% volume loss. The relative differences in pore volume, and their accessibility, are reflected in the BET surface areas of ca. 245 m^2/g for the aerogel relative to 47 m^2/g for the xerogel (with the latter comparable to precipitated CdS nanoparticles). Additionally, the average pore size and cumulative pore volume are considerably larger for the aerogels. An examination of the morphology by TEM clearly shows the particulate nature of the aerogel and the presence of a random mesoporous network (Figure 2B), similar to the morphology of the GeS_2 gels prepared by thiolysis reactions. However, unlike GeS_2 gels, the nanoparticle building blocks within the CdS gels are crystalline, as indicated by X-ray powder diffraction (Figure 3) and adopt the cubic structure, as is the case for the nanoparticles from which the gels are prepared. This is typical for low-temperature CdS nanoparticle synthetic routes. Upon heating, X-ray data suggest the aerogels transform to the more stable hexagonal modification, evident in data collected at $\geq$300°C (Figure 3). However, TEM analyses of a 100°C heated aerogel sample clearly show hexagonal facets (Figure 2C), and the d-spacing values computed from lattice fringes (Figure 2D) and electron diffraction data are also indicative of hexagonal CdS, suggesting the transformation starts at a much lower temperature.[38,39] In addition to the structural change, heating also has a large impact on the primary particle size of the nanoparticle building blocks in the aerogel, presumably due to sintering, and this has a corresponding impact on the extent of quantum confinement, as probed by the absorption onset (Figure 4). The gel-network itself undergoes considerable densification, evidenced by a corresponding decrease in BET surface area (Figure 5).

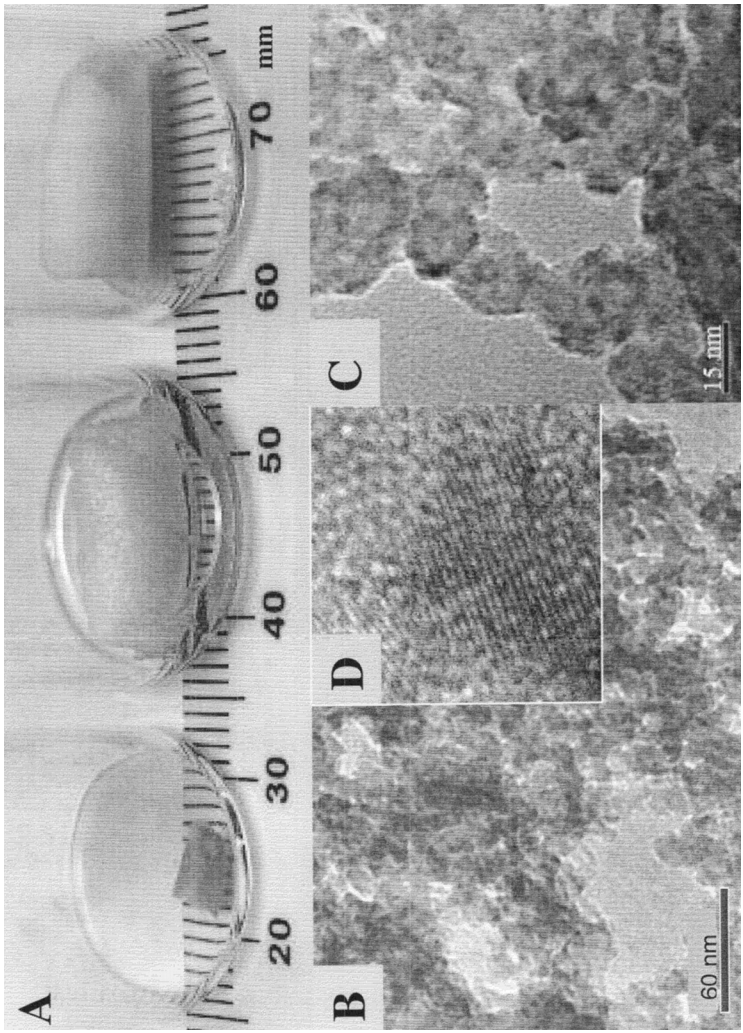

Figure 2. (A) a photograph provides a comparison of a wet CdS gel (center) with an unwashed CdS xerogel (left) and a monolithic CdS aerogel (right). Electron microscope images of CdS aerogels illustrating the particulate nature of the network: (B) as-prepared; (C) after heating in vacuo at 100°C, hexagonal facets are apparent on the particles; (D) a high resolution image of a single particle from B showing lattice fringes with separation distances of 2.5 Å, corresponding to the (102) reflection of hexagonal CdS. Parts A, B, D reproduced with permission from Science **307**, 397 (2005). Part C reproduced with permission from *J. Non-Cryst. Solids* **350**, 1 (2004). Copyright 2004 Elsevier.

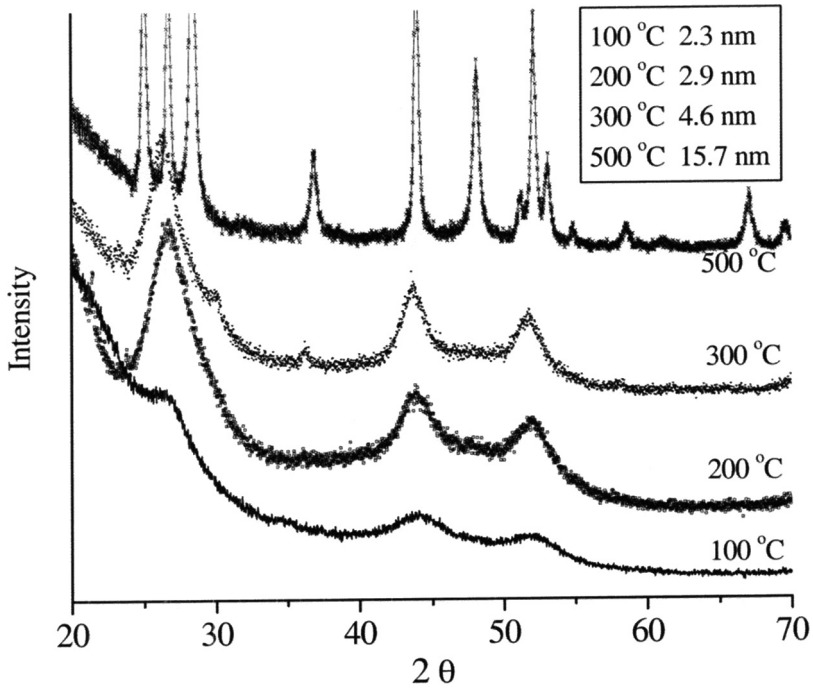

Figure 3. Powder X-ray diffraction patterns of heated CdS aerogels. Prominent peaks seen in the 100, 200, and 300°C sample correspond to the cubic form of CdS (Hawleyite) and those in the 500°C sample correspond to the hexagonal form (Greenockite). The inset shows the particle size calculated using the Scherrer formula at the various heating temperatures. Reproduced with permission from *J. Non-Cryst. Solids* **350**, 1 (2004). Copyright 2004 Elsevier.

In order to independently probe the roles of nanocrystal growth and densification on the quantum confinement effects in the network solid, the optical properties of a CdS xerogel were compared to a corresponding aerogel (Figure 6). The samples are both low-temperature processed, and the crystallite sizes of the primary particle building blocks (as probed by XRD) are essentially identical. However, the optical properties are drastically different, with the more dense xerogel exhibiting an onset near that of bulk CdS (weak quantum confinement) whereas the onset of the less dense aerogel is considerably blue-shifted.[40] This strongly suggests that the extent of quantum confinement in fractal gels is a function of the volume density. The fact that the wet gel and aerogel exhibit similar optical properties (both strongly confined) is a good

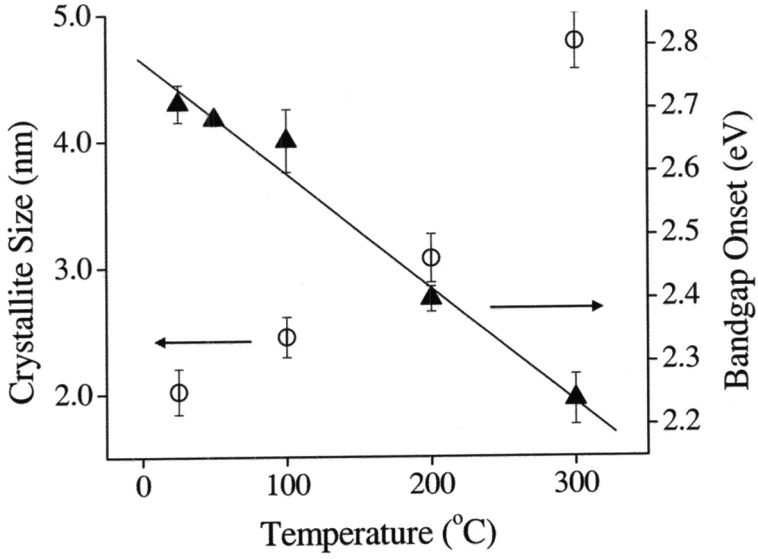

Figure 4. Influence of temperature processing (conducted in vacuo) on crystallite size of the primary particle components in CdS aerogels (○, X-ray powder diffraction data) and on absorption onset of CdS aerogels (▲, diffuse reflectance data). Reproduced with permission from *Science* **307**, 397 (2005).

indicator that the low-dimensional (low-density) framework present in the wet-gel is largely conserved in the aerogel. These data suggest that nanoparticles can be physically linked together (wired) into 3-D functional architectures without compromising the unique opto-electronic effects that are the hallmark of quantum confinement.

Much of the interest in semiconductor nanoparticles (quantum dots) stems from the sharp and intense luminescence features that arise from the discrete, atom-like states. However, the band-edge luminescence is easily quenched by defects within the particle (due to poor crystallinity) or at the surface. These give rise to mid-gap states and corresponding broad features red-shifted from the band-edge. Additionally, photooxidation of the surface can lead to a blue shift in the photoluminescence due to the transformation of the CdSe outer surface to CdO, effectively reducing the size of the quantum dots,[41] and the corresponding passivation of surface trap states can increase the band edge emission intensity.[42] Accordingly, we conducted photoluminescence experiments on the precursor nanoparticles and aerogels as a method to probe the

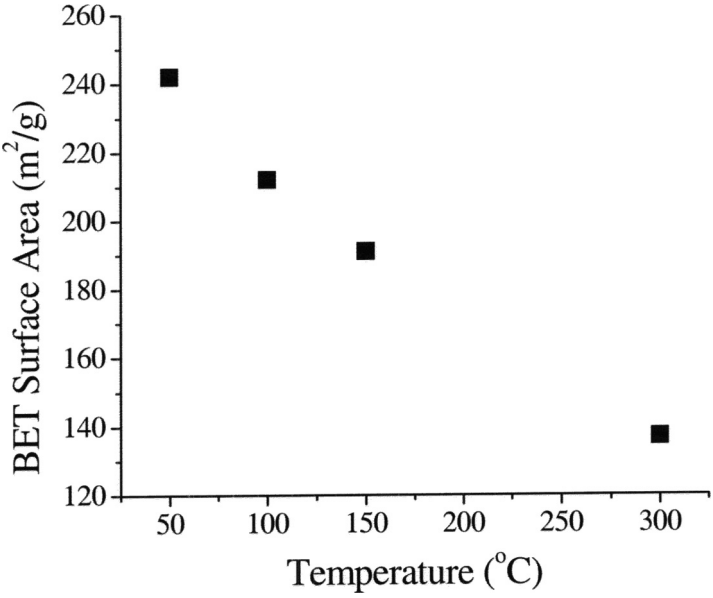

Figure 5. Effect of temperature processing (conducted in vacuo) on BET surface area of CdS aerogels.[39]

impact of gelation conditions on defects (Figure 7). 4-fluorophenylthiolate-capped nanoparticles of CdS exhibit a relatively sharp photoluminescence peak at 450 nm, corresponding to the band edge, and a broad feature centered around 600 nm due to the mid-gap trap states. The relatively poor luminescence intensity is characteristic of the poor crystallinity of the nanoparticle samples, itself a function of the low-temperature synthesis strategy. Additionally, thiolate capping groups are well established to act as sites for non-radiative recombination. As prepared aerogels exhibit a broad peak centered around 550 nm. There is no evidence of a corresponding band-edge emission. However, the band-edge emission can be recovered upon heating in vacuo at 100°C, presumably due to annealing out of some of the defects responsible for non-radiative recombination.[39] Thus, appropriately processed CdS aerogels have the same photoluminescence signature as their discrete nanoparticle building blocks. This further indicates that any CdO formation at the particles' surface is minimal (little passivation of trap states) and does not change during the transformation of nanoparticles to aerogels.

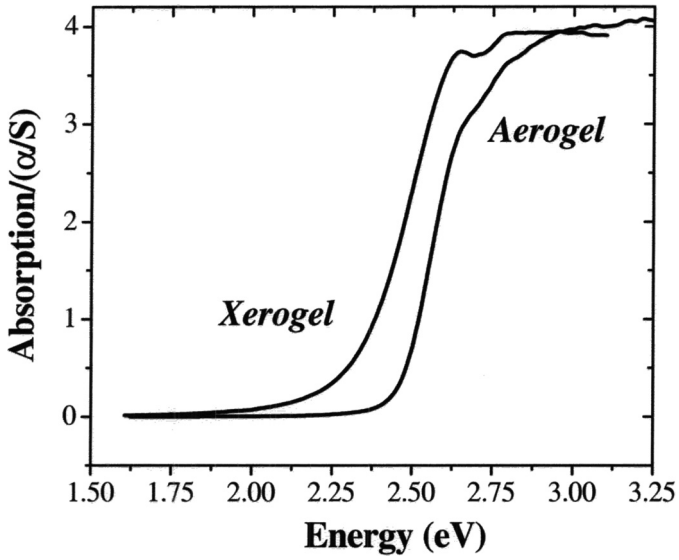

Figure 6. Optical absorbance data (converted from solid state reflectance) for low-temperature processed CdS aerogels and xerogels. The extent of quantum confinement is dependent on the density of the framework, with the more-dense xerogel exhibiting an onset near the bulk value for CdS, whereas the onset for the low-density aerogel is considerably blue-shifted. Reproduced with permission from *Chem. Mater.* **17**, 6644 (2005), online Table of Contents entry. Copyright 2005 American Chemical Society.

Application of the Nanoparticle Condensation Route to Other Metal Chalcogenides

We have shown that the CdS gels reported by Gacoin can be easily transformed into robust xerogels and aerogels. The question remains as to whether this is a general phenomenon, or specific to the CdS system demonstrated by Gacoin. To test the generality of the approach, the ability to form gels, xerogels, and aerogels of PbS, ZnS, and CdSe was probed. ZnS and PbS represent opposite ends of the optical spectrum, with ZnS absorbing in the UV and PbS in the IR. Although red-shifted relative to CdS, CdSe tends to absorb in the visible range when prepared as quantum confined nanoparticles. The nanoparticles were all prepared by low-temperature processing employing reverse microemulsions, capped with 4-fluorophenylthiolate, and treated with H_2O_2 (PbS, ZnS) or tetranitromethane (CdSe). Gels formed in all cases, though only ZnS showed a tendency to form monoliths as observed

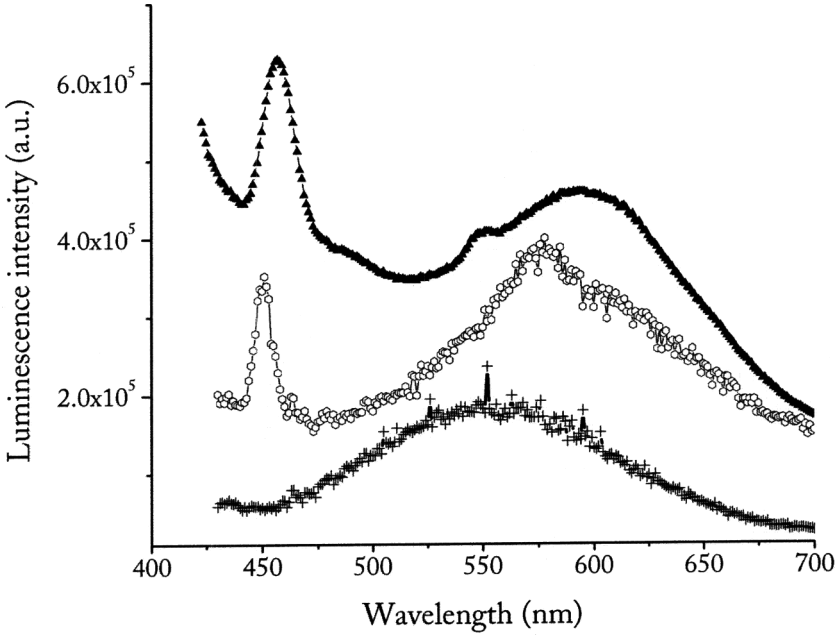

Figure 7. Photoluminescence spectra of capped CdS nanoparticles in solution (▲). Solid state reflectance data (converted to absorbance) of an as-prepared aerogel (+) and a 100°C heated (in vacuo) aerogel (○). The excitation wavelength was 400 nm in each case. Reproduced with permission from *Science* **307**, 397 (2005), supporting online material.

for CdS.[40] The resulting gels were aged for up to two weeks in the mother liquor prior to solvent exchange with acetone to remove byproducts and ambient pressure or CO_2 supercritical drying. In all cases, the resultant aerogels exhibited absorbance onsets that were blue-shifted from those of the corresponding xerogels along with considerably higher surface areas (Table 2), suggesting that the observation of stronger quantum confinement as a function of decreased framework density (dimensionality) observed for CdS is a general phenomenon, as is the oxidation induced metal chalcogenide gelation process.[40] The influence of dimensionality is particularly evident when comparing a series of materials with gradually increasing density, as illustrated for CdSe in Figure 8. Furthermore, in addition to varying the density of the framework, the extent of quantum confinement can also be tuned by varying the primary particle size from which the gel is assembled. Thus, an aerogel prepared from 5.0 nm diameter CdSe nanoparticles has a

Table 2. Bulk band gap values and absorption onsets of xerogel and aerogel samples for the as-prepared PbS, CdSe, CdS, and ZnS materials; BET surface areas of corresponding materials degassed at 100°C for a minimum of 24 hours[38,40]

Metal Chalcogenide	Bulk band gap (eV)	Xerogel band edge (eV)	Aerogel band edge (eV)	Xerogel BET surface area (m^2/g)	Aerogel BET surface area (m^2/g)
CdS	2.45	2.31	2.71	38–55	239–250
PbS	0.37	0.76	0.80	48–57	119–141
CdSe	1.74	1.96	2.19	41–65	128–161
ZnS	3.70	3.77	3.80	29–31	182–202

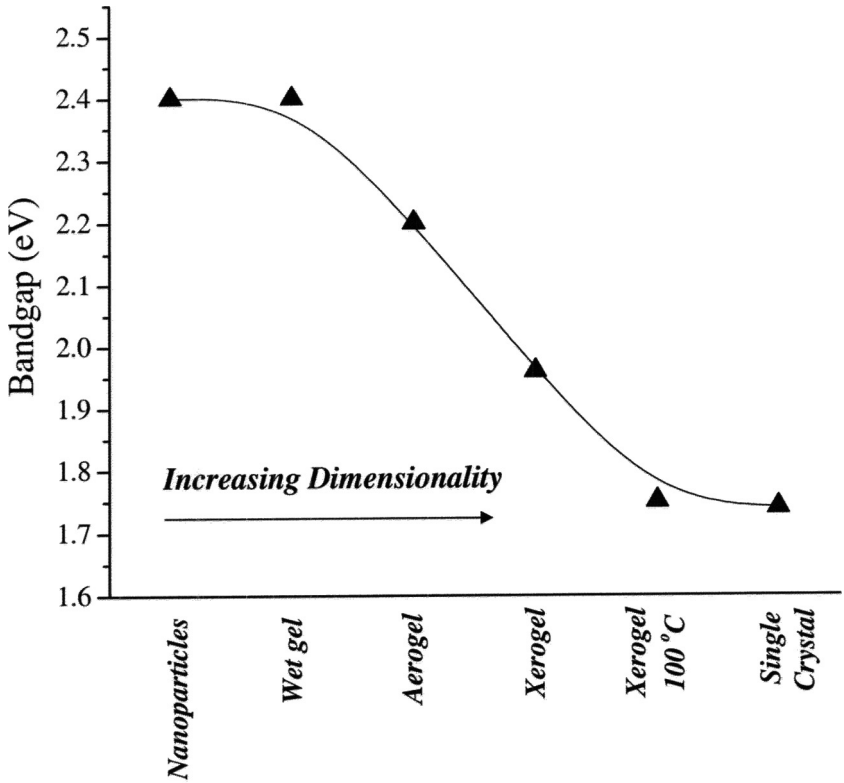

Figure 8. Influence of dimensionality on observed band-edge for CdSe materials: nanoparticles, wet gel, aerogel, xerogel, heated xerogel, and single crystal.[38,40]

decreased band edge of 1.94 eV relative to 2.20 eV for an aerogel prepared from 4.4 nm diameter particles.[38]

Improving Optical Properties in CdSe Aerogels

As indicated above, the weak photoluminescence demonstrated by the aerogel materials is in part a function of the poor crystallinity of the nanoparticle building blocks. That is, aerogels prepared from poorly crystalline (and poorly luminescent) nanoparticles are likely to be poorly luminescent themselves. In order to improve the optical properties, we explored the use of high temperature methods to prepare highly crystalline nanoparticles for gelation. We specifically targeted CdSe because this system is one of the most extensively studied with respect to synthesis and property characterization, and because we think it will be the most promising platform for sensing and photovoltaic devices. Nanoparticles were prepared in the coordinating solvents trioctylphosphine oxide (TOPO) and tetradecylphosphonic acid (TDPA) at 250°C from CdO and Se powder following the method of Peng and Peng[43] The resulting TOPO/TDPA capped particles were observed to fluoresce green under the ambient lighting. Introduction of the thiolate (in this case, mercaptoundecanoic acid, MUA)[44] to the surface resulted in a significant decrease in the band-edge luminescence intensity and formation of a broad shoulder to the red, attributed to the mid-gap states of the thiolate. As-prepared aerogels from MUA-capped CdSe nanoparticles also exhibit the band-edge and mid-gap state luminescence feature seen in the precursor nanoparticles (Figure 9). The latter is more intense in the aerogel relative to the nanoparticles and is considerably red-shifted, suggesting the surface characteristics of the aerogel are different from those of the nanoparticles.[40] Nevertheless, the data bear out the premise that the photoluminescence characteristics of the aerogel are largely determined by those of the nanoparticle building blocks.

Interestingly, gelation of CdSe was found to occur even in systems where no oxidant was introduced, presumably due to photo-induced reactions with O_2 under ambient conditions.[38] Indeed, Gacoin and co-workers have noted that CdS gels were initially formed by air oxidation under room light[32] and Peng and co-workers noted the instability of MUA-capped CdSe to photo-aggregation in air.[44] These data support the notion that oxidation induced gelation is a general approach for nanoparticle assembly that is suitable for a range of materials and experimental conditions.

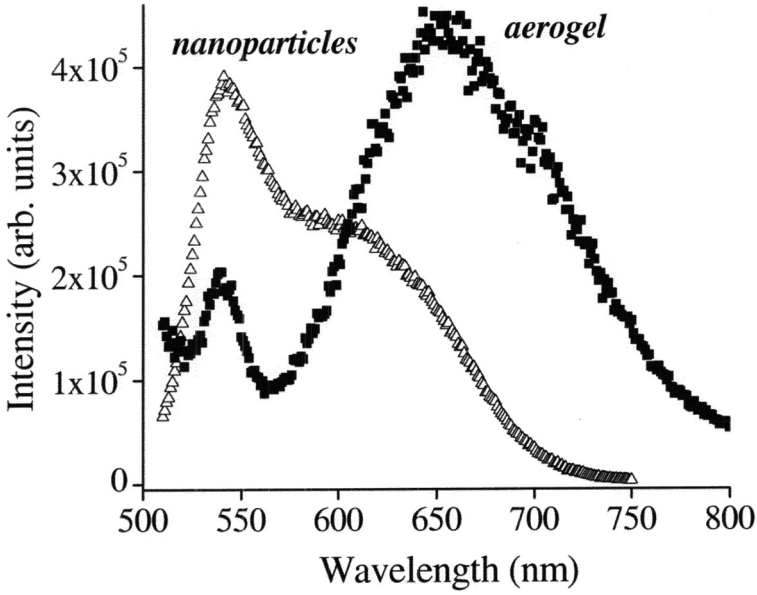

Figure 9. Photoluminescence data for MUA-capped CdSe nanoparticles prepared by the high temperature route (△) and an as-prepared aerogel (■) acquired by using an excitation wavelength of 480 nm. Data were collected at 77 K on powdered aerogel samples sealed under vacuum in a quartz tube. Reproduced with permission from *Science* **307**, 397 (2005).

CONCLUSIONS AND PROSPECTUS

Sol-gel processing provides a powerful and general approach for the creation of porous 3-D nanoarchitectures of metal chalcogenides. Two general approaches have been explored. Nanoparticle condensation strategies separate out the steps involved in primary particle formation and aggregation, and lead exclusively to particulate gels, whereas thiolysis/condensation of molecular components can produce polymeric or particulate gels, or simple precipitates, depending on the kinetics of the individual steps. The density of the gel frameworks (as reflected by the surface area) can be effectively tuned by controlling the drying method, with supercritical drying producing the lowest density materials (aerogels). It is interesting to note that among the materials presented in this Comment, it is the particulate aerogels of GeS_2, prepared by thiolysis strategies, which yield the highest surface areas. Further studies are underway to elucidate whether the high degree of porosity is a

consequence of the gelation method (thiolysis vs. nanoparticle condensation), or is a function of the chemical system under investigation.

The application of sol-gel strategies to metal chalcogenides represents a powerful strategy for the assembly of nanoparticles into functional architectures. In contrast to other techniques for preparing nanoparticle assemblies, such as colloidal crystallization, there is no intervening ligand between the primary particle components. Yet, despite the absence of the confining ligand sphere, quantum confinement effects are retained in the network, with the extent of confinement controlled by the density of the gel. The combination of porosity with the optoelectronic activity of the network should be suitable for the design of novel sensing, catalytic, and photovoltaic devices, avenues that we are presently exploring. Finally, it is worth noting that the general mechanism of gelation, the formation of limited active sites on primary molecular or particle components that then connect in a network fashion throughout the solvent volume, should be chemically versatile; that is, gel formation can be anticipated for a wide range of chemical compositions heretofore unexplored.

ACKNOWLEDGEMENTS

Funding for this work was provided by the National Science Foundation (CAREER: DMR-0094273), Research Corporation (Research Innovation Award R10617) and the Donors of the Petroleum Research Fund administered by the American Chemical Society (PRF-AC 43550).

REFERENCES

1. Weller, H., 1993. *Angew. Chem. Int. Ed. Engl.*, **32**, 41–53.
2. Puentes, V. F., K. M. Krishnan, and A. P. Alivisatos, 2001. *Science*, **291**, 2115–2117.
3. Brinker, C. J. and G. W. Scherer, 1990. *Sol-Gel Science*, Academic Press, San Diego, California.
4. Rolison, D. R. and B. Dunn, 2001. *J. Mater. Chem.*, **11**, 963–980.
5. Hüsing, N. and U. Schubert, 1998. *Angew. Chem. Int. Ed. Engl.*, **37**, 22–45.
6. Melling, P. J. 1984. *Am. Ceram. Soc. Bull*, **63**, 1427–1429.
7. Stanić, V., T. H. Etsell, A. C. Pierre, and R. J. Mikula, 1997. *Mater. Lett.*, **31**, 35–38.
8. Carmalt, C. J., C. W. Dinnage, and I. P. Parkin, 2000. *J. Mater. Chem.*, **10**, 2823–2826.
9. Sriram, M. A. and P. N. Kumta, 1998. *J. Mater. Chem.*, **8**, 2441–2451.

10. Kistler, S. S. 1931. *Nature*, **127**, 741.
11. Kistler, S. S. 1932. *J. Phys. Chem.*, **36**, 52.
12. Sriram, M. A., K. S. Weil, and P. N. Kumta, 1997. *Appl. Organomet. Chem.* **11**, 163–179.
13. Kumta, P. N. and S. H. Risbud, 1993. *Mater. Sci. Eng. B.*, **B18**, 260–268.
14. Kumta, P. N. and S. H. Risbud, 1993. *J. Mater. Res.*, **8**, 1394–1410.
15. Sriram, M. A. and P. N. Kumta, 1998. *J. Mater. Chem.*, **8**, 2453–2463.
16. Carmault, C. J., C. W. Dinnage, I. P. Parkin, A. J. P. White, and D. J. Williams, 2002. *Inorg. Chem.*, **41**, 3668–3672.
17. Allen, G. C., M. Paul, and M. Dunleavy, 1992. *Adv. Mater.*, **4**, 424–427.
18. Purdy, A. P., A. D. Berry, and C. F. George, 1997. *Inorg. Chem.*, **36**, 3370–3375.
19. Stanić, V., A. C. Pierre, T. H. Etsell, and R. J. Mikula, 1997. *J. Non-Cryst. Solids*, **220**, 58–62.
20. Seisenbaeva, G. A., S. Gohil, K. Jansson, K. Herbst, M. Brorson, and V. G. Kessler, 2003. *New J. Chem.*, **27**, 1059–1064.
21. Aggarwal, I. D. and J. S. Sanghera, 2002. *J. Optoelec. Adv. Mater*, **4**, 665–678.
22. Martins, O., J. Xu, and R. M. Almeida, 1999. *J. Non-Cryst. Solids*, **256 & 257**, 25–30.
23. Seddon, A. B., S. N. B. Hodgson, and M. G. Scott, 1991. *J. Mater. Sci.*, **26**, 2599–2602.
24. Stanić, V., A. C. Pierre, and T. H. Etsell, 1996. *J. Mater. Res.*, **11**, 363–372.
25. Stanić, V., A. C. Pierre, T. H. Etsell, and R. J. Mikula, 2000. *J. Am. Ceram. Soc.*, **83**, 1790–1796.
26. Stanić, V., A. C. Pierre, T. H. Etsell, and R. J. Mikula, 2001. *J. Phys. Chem. A*, **105**, 6136–6143.
27. Stanić, V., T. H. Etsell, A. C. Pierre, and R. J. Mikula, 1997. *J. Mater. Chem.*, **7**, 105–107.
28. Sanghera, J. S., C. Scotto, S. Bayya, and I. D. Aggarwal, 1999. *J. Non-Cryst. Solids*, **256 & 257**, 31–35.
29. Kalebaila, K. K., D. C. Georgiev, and S. L. Brock, 2006. *J. Non-Cryst. Solids*, **352**, 232–240.
30. Hollingsworth, J. A. and V. I. Klimov, 2004. "Soft" chemical synthesis and manipulation of semiconductor nanocrystals. In *Semiconductor and Metal Nanocrystals: Synthesis and Electronic and Optical Properties*, Klimov, V. I., (ed.), pp. 1–64, Marcel Dekker, New York.
31. Gacoin, T., L. Malier, and J.-P. Boilot, 1997. *J. Mater. Chem.* **7**, 859–860.
32. Gacoin, T., L. Malier, and J.-P. Boilot, 1997. *Chem. Mater*, **9**, 1502–1504.
33. Gacoin, T., K. Lahlil, P. Larregaray, and J.-P. Boilot, 2001. *J. Phys. Chem. B*, **105**, 10228–10235.
34. Capoen, B., T. Gacoin, J. M. Nédélec, S. Turrell, and M. Bouazaoui, 2001. *J. Mater. Sci.*, **36**, 2565–2570.

35. Malier, L., J.-P. Boilot, and T. Gacoin, 1998. *J. Sol-Gel Sci. Tech.*, **13**, 61–64.
36. Yu, H., J. Li, R. A. Loomis, P. C. Gibbons, L.-W. Wang, and W. E. Buhro, 2003. *J. Am. Chem. Soc.*, **125**, 16168–16169.
37. Yu, H., J. Li, R. A. Loomis, L.-W. Wang, and W. E. Buhro, 2003. *Nature Mater*, **2**, 517–520.
38. Mohanan, J. L., I. U. Arachchige, and S. L. Brock, 2005. *Science*, **307**, 397–400.
39. Mohanan, J. L., and S. L. Brock, 2004. *J. Non-Cryst. Solids*, **350**, 1–8.
40. Arachchige, I. U., J. L. Mohanan, and S. L. Brock, 2005. *Chem. Mater*, **17**, 6644–6650.
41. Van Sark, W. G. J. H. M., P. L. T. M. Frederix, M. A. H. Asselbergs, and D. J. Van den Heuvel, A. Meijerink, and H. C. Gerritsen, 2002. *Springer Series on Fluorescence, 2 (Fluorescence Spectroscy, Imaging and Probes)*, 317–335.
42. Javier, A. and G. F. Strouse, 2004. *Chem. Phys. Lett.*, **391**, 60–63.
43. Peng, Z. A. and X. Peng, 2001. *J. Am. Chem. Soc.*, **123**, 183–184.
44. Aldana, J., Y. A. Wang, and X. Peng, 2001. *J. Am. Chem. Soc.*, **123**, 8844–8850.